Imparting Superhydrophobicity with a Hierarchical Block Copolymer Coating

Citation: Cheng, Li#Chen, Simonaitis, John W., Gadelrab, Karim R., Tahir, Mukarram, Ding, Yi et al. 2019. "Imparting Superhydrophobicity with a Hierarchical Block Copolymer Coating." Small, 16 (1).

As Published: http://dx.doi.org/10.1002/smll.201905509

Publisher: Wiley

Persistent URL: https://hdl.handle.net/1721.1/140781

Version: Original manuscript: author's manuscript prior to formal peer review

Imparting Superhydrophobicity with a Hierarchical Block Copolymer Coating

Li-Chen Cheng[1*], *John W. Simonaitis*[2*], *Karim R. Gadelrab*[1], *Mukarram Tahir*[1], *Yi Ding*[1], *Alfredo Alexander-Katz*[1], *and Caroline A. Ross*[1]

[1]Department of Materials Science and Engineering and [2]Department of Electrical Engineering and Computer Science, Massachusetts Institute of Technology, Cambridge, MA, 02139, USA

*Author Contributions:

L.C. and J.S. contributed equally.

Email:

clichen@mit.edu

johnsimo@mit.edu

karimgad@mit.edu

mtahir@mit.edu

yding@mit.edu

aalexand@mit.edu

caross@mit.edu

ABSTRACT

A robust and transparent silica-like coating that imparts superhydrophobicity to a surface through its hierarchical multilevel self-assembled structure is demonstrated. This approach involves iterative steps of spin-coating, annealing, and etching of polystyrene-*block*-polydimethylsiloxane block copolymer thin films to form a tailored multilayer nanoscale topographic pattern with a water contact angle up to 155˚. A model based on the hierarchical topography was developed to calculate the

wetting angle and optimize the superhydrophobicity, in agreement with the experimental trends, and explaining superhydrophobicity arising through combination of roughness at different lengthscales. Additionally, the mechanical robustness and optically passive properties of the resulting hydrophobic surfaces were demonstrated.

KEYWORDS

Block copolymer, Self-assembly, Hierarchical structure, Superhydrophobicity, Wetting behavior

Superhydrophobic surfaces are defined by their characteristic ability to repel water and the resulting resistance to wetting,[1–4] and can be created by introducing appropriate surface roughness and chemical functionalization. Superhydrophobicity is alternatively called the lotus effect because it underlies the self-cleaning ability of the lotus plant and certain insect wings.[5–10] Quantitatively, superhydrophobicity corresponds to a water contact angle that exceeds 150° and a roll-off angle less than 10°.[11,12], The large contact angle reduces the contact area between a water droplet and the surface, and allows the droplet to roll off at a small tilt angle. As a result, the water droplet will dislodge hydrophilic contaminants from the surface, making the surface self-cleaning. In addition, the continuous condensation and roll-off of water from a surface improves heat transfer through the interface.[13] Superhydrophobic surfaces therefore hold technological promise for a myriad of applications including anti-fouling, reduced drag-force on ships, combustion engines, heat exchangers, synthetic fibers, windshields, solar panels, airplanes, and droplet transfer in microfluidics.[14–17] More generally, water-surface interactions are central to the performance of a vast range of critical technologies including membranes, sensors and sorbent materials, spanning different environments, service conditions and length scales.[18]

Recent studies suggest that multiscale roughness is beneficial for the enhanced superhydrophobicity displayed by many natural surfaces.[19–23] Synthetic analogues of superhydrophobic surfaces have been prepared by introducing micro-scale features onto a surface in order to generate the necessary roughness for trapping air under a water droplet.[4],[8],[24] A variety of surface coatings have been

produced using lithography, nanoimprint, chemical synthesis chemical vapor deposition, nanoparticle coating and other procedures.[25–29],29,30,31 For example, chemical vapor deposition was used to produce a thin-film of titanium dioxide on self-cleaning glass,[30] and glasses used for windshield or rear-view mirrors have been imparted with hydrophobicity by wet-coating organic compounds or hybrid composites.[31] Important considerations for superhydrophobic surfaces are abrasion resistance, which is often limited by the adhesion strength of the coating,[32] and optical properties, i.e. ensuring that the roughness does not compromise the optical qualities of the surface and restrict its utility in applications such as solar cell panels and window treatments.[33] The reduced optical transparency of the roughened surfaces is due to Mie scattering from features of similar size to the wavelength,[34] in which the scattering intensity increases rapidly with the ratio of the characteristic surface features to the wavelength of light. Sub-100 nm roughness is therefore preferable to enhance the optical transparency for visible light.[17],[28,29],[35–37] This motivates the search for processes that can produce robust, transparent superhydrophobic surfaces.

Block copolymers (BCPs) self-assemble into periodic nanoscale patterns with controllable size and morphology determined by the molecular weight and composition of the BCP.[38],[39] The resulting self-assembled features can themselves be functional, or can be employed as a mask to pattern other functional materials.[40] BCPs have been used to pattern surfaces to achieve hydrophobicity,[41–45] for example, silica nanopillar arrays with 100 nm period were fabricated using micellar films of polystyrene-block-poly(2-vinylpyridine) as etch masks. The height, radius, and periodicity of the nanopillar arrays were varied by tuning the deposition and plasma etching conditions, and the high water repellency originated from the resulting surface roughness.[43] Cylindrical pillars and nanocones with feature spacing less than 100 nm were patterned in Si using a mask made from a polystyrene-block-poly(methyl methacrylate) (PS-*b*-PMMA) film in which aluminum oxide was selectively incorporated in the PMMA domains by sequential infiltration synthesis. The textured surface rendered a substantial improvement in the surface wetting properties, and its robustness was investigated by means of high-speed water droplet impingement.[45] Coatings with micron-scale roughness formed by vapor-induced phase separation of a block copolymer also enhanced superhydrophobicity.[44] However, the self-assembled microdomains from block copolymers composed of organic monomers display poor mechanical stability and etching selectivity, necessitating additional pattern transfer steps to achieve final robust surface features, accomplished, for example, by a damascene processes,[46] lift-off,[47] or sequential infiltration

synthesis.[45] Additionally, many of these works have focused on creating a monolayer of self-assembled nanoscale features with a uniform period. Block copolymer self-assembly has the potential to make hierarchical surfaces at sub-100 nm length with multiple precisely-controlled length scales and geometries, and it is therefore of interest to synthesize such surfaces and realize the predicted improvements in hydrophobic behavior.

Herein, we report a method for functionalizing a surface with a durable and optically passive hydrophobic coating via the self-assembly of silicon-containing BCPs. An iterative process of spin-coating, annealing, and etching of cylindrical-forming polystyrene-*block*-polydimethylsiloxane (PS-*b*-PDMS) thin films was employed to manufacture multilayer hierarchical structures. An oxygen plasma treatment removes the PS block and transforms the PDMS block into robust silica-like line patterns forming immobilized topographical features without requiring further pattern transfer processes.[48] The inherent tunability of the geometric characteristics of the multilayer topography also facilitates systematic studies of surface wetting behavior at the nanoscale. To understand how superhydrophobicity emerges from multilayer hierarchical BCP structures, a topographical model was constructed, and the apparent water contact angles of various mesh and grating structures were simulated. The results reveal the significance of controllably introducing multiple well-defined levels of patterning through the self-assembly block copolymer method.

The wetting behavior of surfaces has long been understood as the result of surface tension between water, air, and the surface in question (in this case, the etched BCP). From the work of Cassie and Baxter[1] to that of Calvimontes,[49] the calculation, modeling, and simulation of wetting on arbitrary surfaces has become well established. We applied these theories to simulate the relative wetting behavior of water on hierarchical BCP line and mesh patterns with varying length scales and layer alignment as described in the Methods section. These structures were based on the observed geometries of multilayered BCP films, where sequential deposition, annealing and etching of BCP films leads to either parallel alignment of cylinders, or the spontaneous orthogonal ordering of one layer of in-plane cylinders on another to form mesh patterns.[50] The topography is modeled as meshes or gratings of smoothly curved approximately hemicylindrical structures with different periods and orientations. The layers of in-plane cylinders in the hierarchical structures are labelled as A, B and C, with A having the largest period of 80 nm, B a period of 40 nm and C a period of 20 nm,

and the symbols ∨, ⊥, and ∥ refer to angled, orthogonal, and parallel alignments of the cylinders in successive layers. Several structures and their labels are shown in Figure 1(a) and a comparison of model and experimental topography is shown in Figure S1.

To calculate the wetting behavior, water is placed on the model topography, making contact at a height of *h* above the plane of the substrate. Air is trapped in the recesses of the topography below *h*, and the total interfacial energy consists of contributions from the liquid-solid and the liquid-air interfaces. By calculating the energy as a function of *h*, the equilibrium configuration and energy of the wetted interface is determined from which the contact angle is found. This analysis neglects gravity and the effects of captured air pressure in the cavities, and assumes insoluble surfaces, homogenous hydrophobic coatings on all surfaces, and complete BCP coverage.[49]

Table 1. Predicted contact angles of block copolymer structures.

Structure	Predicted Wetting Height[b]	Predicted Contact Angle
Smooth (No Coating)[a]	0 nm	40° (Measured)
Smooth	0 nm	120°
A (No Coating)	0 nm	10°
A	None[c]	130° - 150°
A ⊥ B	22 nm	162°
A ∨ B	22 nm	162°
A ∥ B	13 nm	148°
A || B ⊥ C	20nm	164°
A ⊥ B ⊥ C	30 nm	170°

[a]No coating refers to the absence of the hydrophobic fluorosilane brush layer. [b]Predicted height refers to the calculated equilibrium height of the water contact line above the plane of the substrate. [c]For this topography no stable height was found.

The results of the analysis of the structures in Figure 1(a) are summarized in Table 1, revealing several important trends that can be used to understand the influence of nanoscale topography on hydrophobicity. The first observation is that introducing any roughness to the surface, even a grating

pattern made from a single layer of a BCP dramatically increases the contact angle of a brush-layer-coated surface. However, there is no predicted thermodynamic stable state for wetting of a surface consisting of a single layer grating pattern, and instead we predict a range of wetting values. The second observation is that adding layers of different length scales always improves hydrophobicity, regardless of the orientation. This is seen in comparing the wetting angles on a single layer of A to the results of A ⊥ B, A ∨ B, and A ∥ B. It is not necessary for the second layer to have a smaller period than the first, and structures such as B ⊥ A and A ⊥ A also increase the wetting angle compared to that of A. In practice, fabrication of B ⊥ A and A ⊥ A structures was more challenging due to poorer surface coverage and orthogonality of the upper layer with respect to the lower layer. The third observation is that orthogonal alignment of the cylinders to form a mesh leads to greater hydrophobicity than that obtained from parallel cylinders. The orthogonal topographical structures are able to pin the droplets at higher points above the surface and maximize the liquid-air surface contact while minimizing contact with the topography. The 45° and 90° orientations had similar wetting angles. Three-layer structures, A ⊥ B ⊥ C and A ∥ B ⊥ C, showed the same trends and offered a further increase in the predicted wetting angle.

The theoretical results were used as a guide in the preparation of superhydrophobic BCP films on glass substrates. Figure 1(b) outlines the manufacturing process utilized to fabricate A ∥ B ⊥C as an example. To prepare multilayer hierarchical nanostructures, the first layer of BCP was spin-coated, solvent annealed and etched in oxygen to form a topographical silica-like grating pattern. A second BCP was then spin-coated, annealed and etched, followed by a third BCP, and the final structure was treated with a hydrophobic brush layer. Self-consistent field theory showed that orthogonal alignment of the second layer of cylinders with respect to the first is promoted if the lower surface has shallow topography or weak affinity to either of the two blocks, independent of the trench spacing. On the other hand, a parallel alignment is favored for deeper topography when the domain spacing between the two BCP layers is close to commensurate. This is particularly true when the substrate surface is attractive to the majority block.[50–52] Further information regarding BCP sample preparation, hydrophobic brush treatment, contact angle measurement, as well as optical and mechanical characterizations is given in the Methods section.

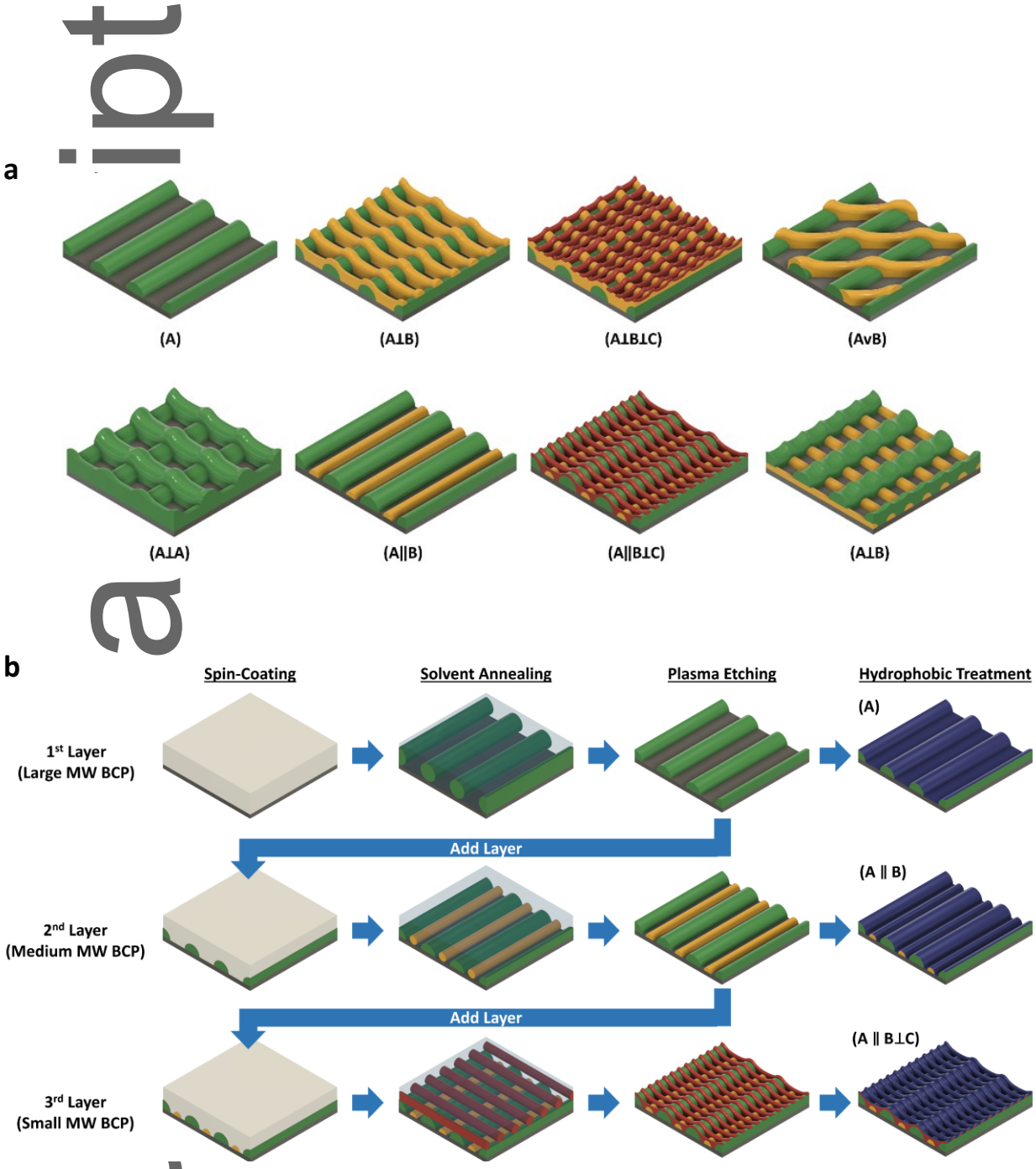

Figure 1. (a) Schematic examples of hierarchical BCP structures. The label A refers to the block copolymer with the largest period shown in green, B to the intermediate period in yellow, and C to the smallest period in red. The ordering from left to right refers to the order in which they were deposited, i.e. the first letter is the bottom layer, and the symbols V, ⊥, and ‖ refer to angled, orthogonal, and parallel alignments of the cylinders. (b) The fabrication process for multi-layer

hierarchical structure A ‖ B ⊥C. Each block copolymer film is spin-coated, solvent annealed, and etched, and the process is repeated to form a hierarchical structure.

Three different cylinder-forming PS-*b*-PDMS BCPs were used in the experiments with total number average molecular weight (M_n) of 123 kg mol^{-1} (labeled SD123; fraction of PDMS f_{PDMS} = 0.38, period L_0 = 80 nm), 53 kg mol^{-1} (SD53; f_{PDMS} = 0.30, L_0 = 40 nm), and 16 kg mol^{-1} (SD16; f_{PDMS} = 0.32, L_0 = 20 nm). The silica-like topographic structures produced by etching the BCP are hydrophilic, and a hydrophobic brush layer was therefore applied, either hydroxy-terminated PDMS or a perfluorosilane coating, (heptadecafluoro-1,1,2,2,-tetrahydrodecyl)trichlorosilane. The contact angle of untreated glass substrate was measured as a reference, showing a low contact angle of 43°, increasing to 93° on application of the PDMS brush layer and 114˚ for the perfluorosilane brush layer, as shown in Figures 2(a) and 3(a).

A topography consisting of a hierarchical pattern of parallel cylinders made from SD123 as the first layer and SD53 as the second layer with a PDMS brush layer is presented in Figure 2(b). This A || B structure had a contact angle of approximately 112°, i.e. the topography increased the wetting angle by 19˚. A perfluorosilane-coated A || B ⊥ C topography with SD123 as the first layer, SD53 as the second layer, and SD16 as the third layer, Figure 3(b), showed a contact angle of 155˚ (vs. 114° for the perfluorosilane-coated glass) and a roll-off angle of 20˚. These results confirm the beneficial results of the multilayer hierarchical topography in increasing the contact angle. We also tested other structures such as A ⊥ C ⊥ B and A ⊥ C ⊥ C which produced hydrophobic results as shown in Figure S2, 147˚ and 148˚ respectively.

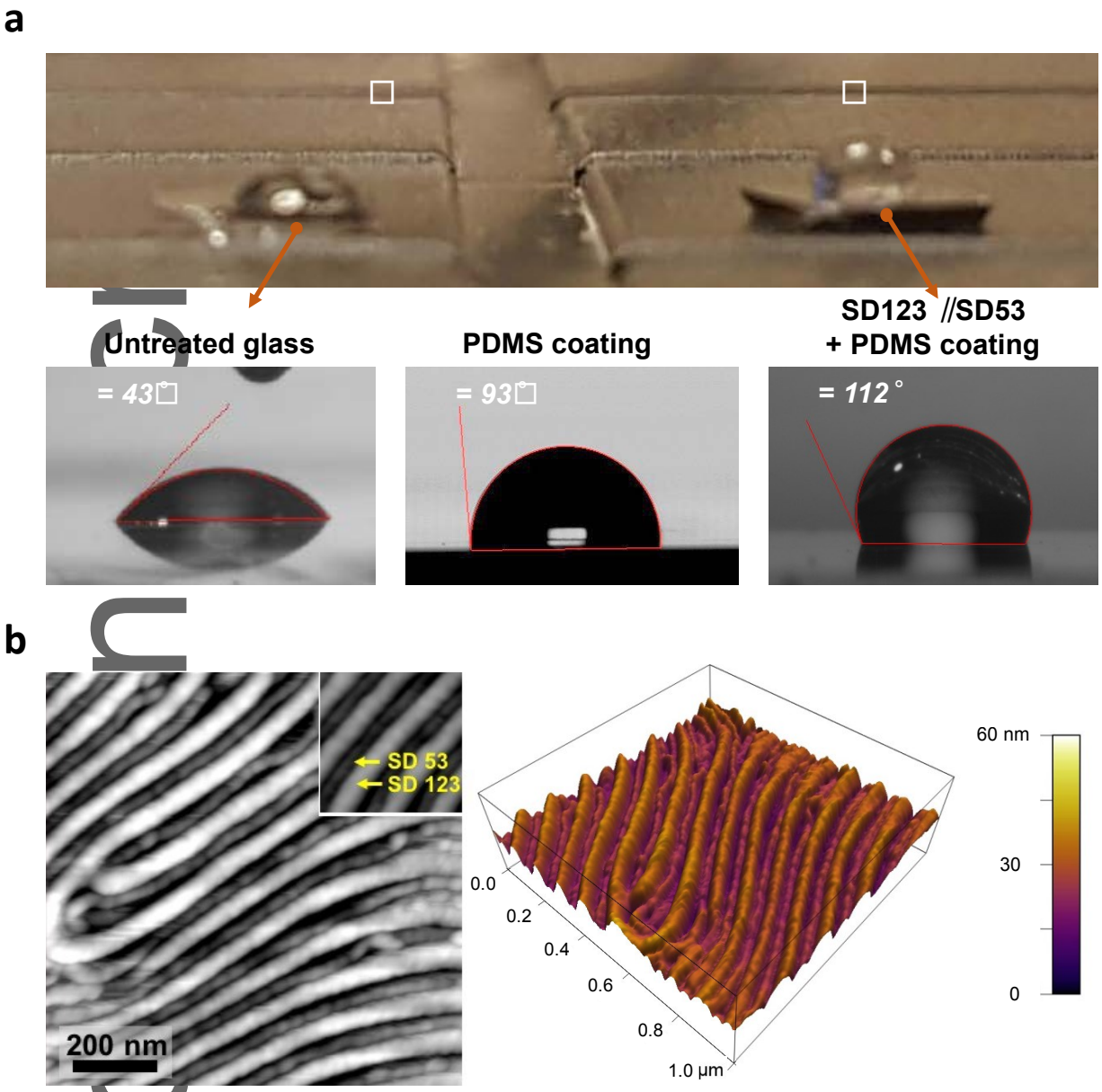

Figure 2. (a) Contact angles of untreated, PDMS-coated, and PDMS-coated bilayer-patterned glass substrate. (b) AFM topography images of the bilayer A ‖ B (SD123 ‖ SD53) surface.

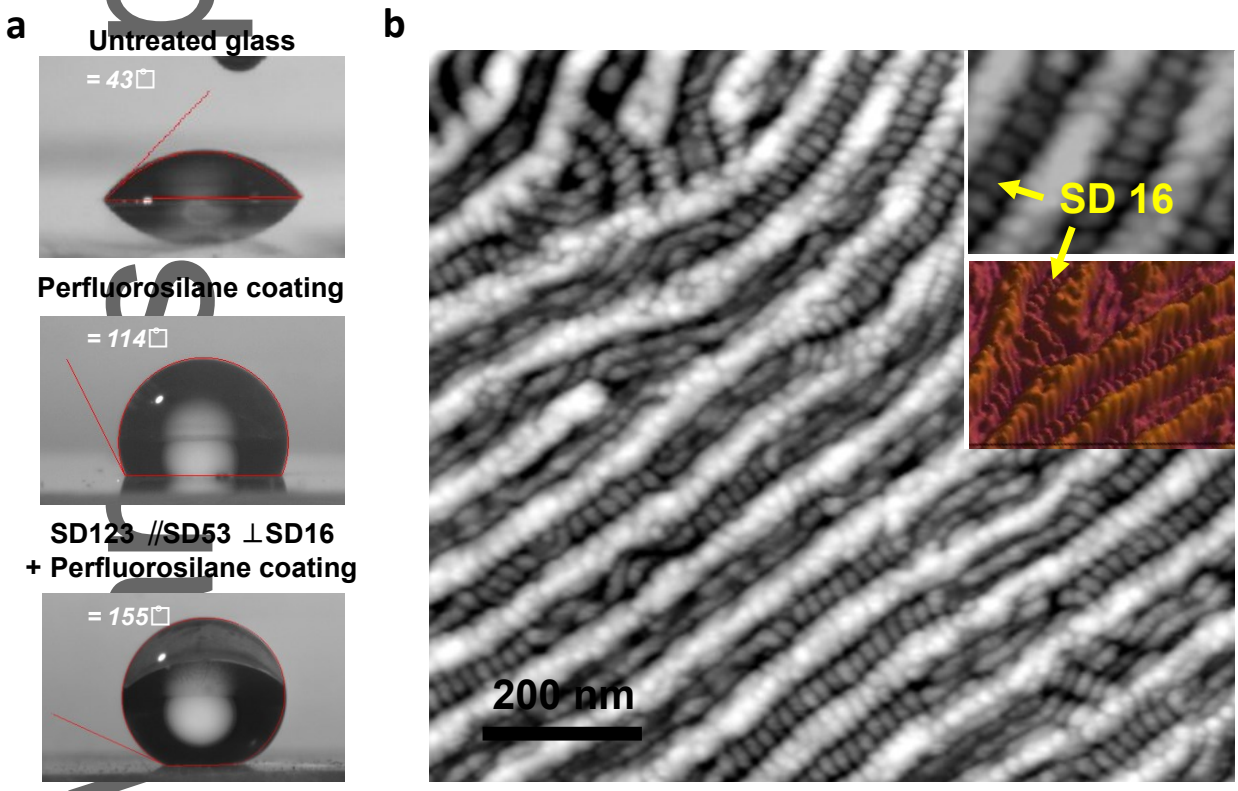

Figure 3. (a) Contact angles of untreated, perfluorosilane-coated, and perfluorosilane-coated tri-layer-patterned glass substrate. (b) AFM topography images of the tri-layer (SD123 ∥ SD53 ⊥ SD16) BCP film. The inset shows a section of a 3D perspective image, scale as in Fig. 2b.

The optical and mechanical characterizations of the hydrophobic surfaces are shown in Figure 4. The optical transmittance of a hydroxy-terminated PDMS coated glass film, Figure 4(a), shows negligible difference with respect to the reference substrate (air and bare glass), with an average of 92.36% transmittance over the visible wavelength ranging from 380 to 740 nm.[26] The transmittance obtained for a superhydrophobic surface composed of a tri-layer (SD123 ∥ SD53 ⊥ SD16) with a PDMS brush layer was 1.4 ± 0.4 % lower than that of reference substrate over the visible wavelength range, in line with transparency measurements for other substrates treated with

nanoscale patterning for superhydrophobicity[53–55]. The absorption of visible light by the patterned glass substrates is low because the length scale of the roughness is significantly lower than the wavelength of visible light. On the other hand, the mechanical robustness of the plasma oxidized-PDMS patterns on the glass was examined by an adhesion test (Figure S3) in which an adhesive tape was pressed onto the surface with a steel roller then peeled off.[56] The RMS surface roughness of a single-layer surface SD53 decreased from an initial value of 3.73 nm to 2.85 nm after 100 peel-off cycles, while the topography of the BCP structures on the glass film remained unchanged, shown in Figure 4(b). The result demonstrates that our etched-BCP coatings preserve their surface topography after multiple repetitive cycles of 90 degree peel adhesion testing.

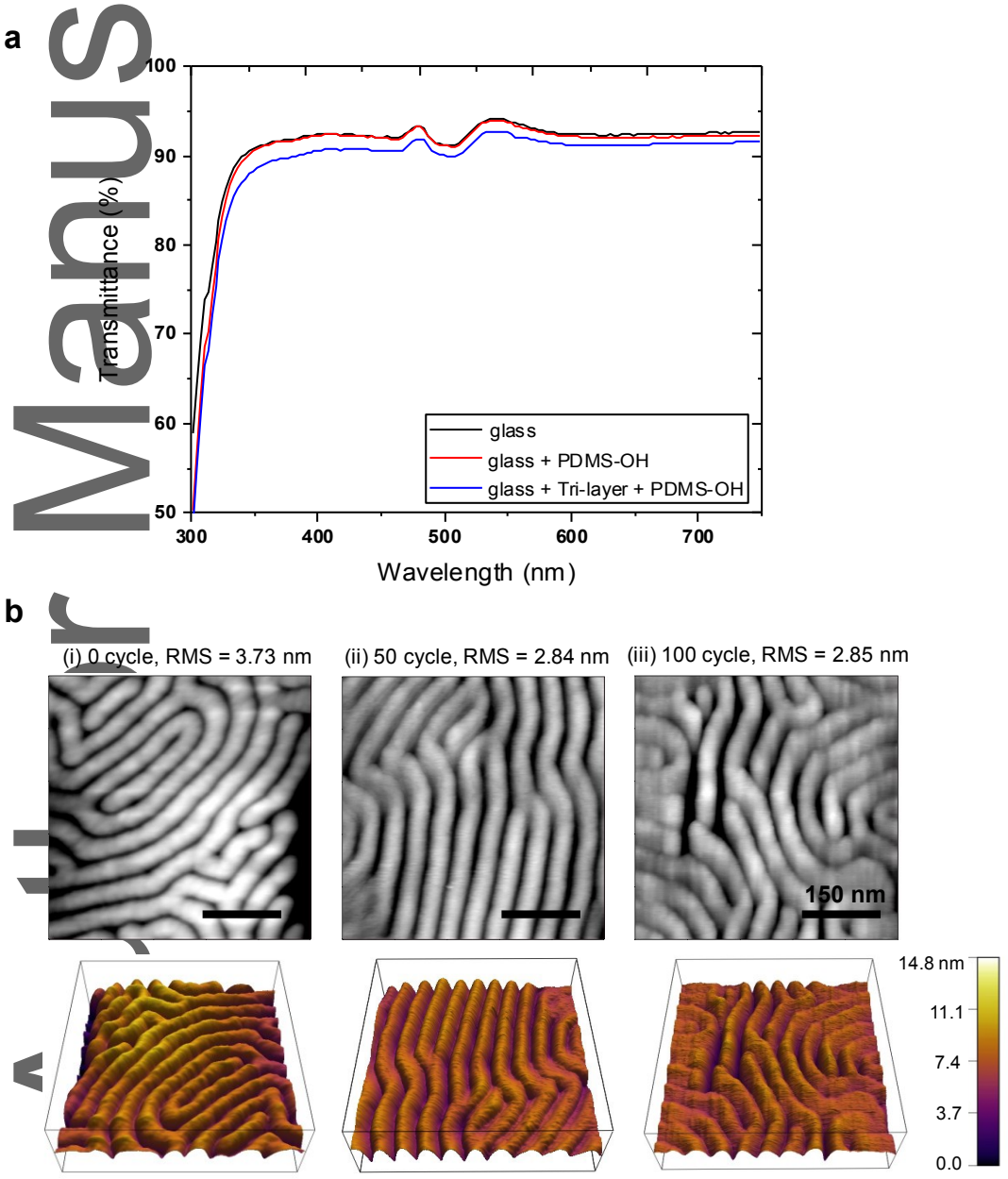

Figure 4. Optical transparency and mechanical robustness test of etched BCP films. (a) Optical transmittance spectrum of reference substrate (air and bare glass), PDMS-brush coated glass, and PDMS-coated tri-layer-patterned glass substrate, showing average transmittance of 92.56%, 92.36%, and 91.23% respectively over the visible wavelength ranging from 380 to 740 nm. (b) AFM topography images of an etched SD53 film subjected to 0, 50 and 100 repetitive peel-off cycles.

In summary, we report a method of imparting superhydrophobicity to a surface through the self-assembly of BCPs to produce a mechanically robust surface with nanoscale hierarchical topography, preserving the optical transparency of the underlying material. The multilevel topography introduces the necessary roughness on the nanoscale to trap air and increase the hydrophobicity of the surface, and can be controlled via the period and layer sequence of the block copolymers. A theoretical model was constructed that predicted wetting angles that followed the trends seen in the experimentally observed topography. By determining the energy for different wetting configurations, the contact angles were calculated. The modelling predicted increasing hydrophobicity in hierarchical structures as observed in the experimental results, especially where the layers of topographical features produced from the BCP align orthogonally or at an angle to form a mesh. A bilayer topography increased the wetting angle from 93° for PDMS-coated glass to 112° for a PDMS-coated bilayer, and from 114° for perfluorosilane-coated glass to 155° for a perfluorosilane-coated tri-layer topography. The superhydrophobic property induced by hierarchical BCP nanostructures presented here lays the foundation for design of robust superhydrophobic coatings which can potentially be fabricated via scalable process such as spray- and dip-coating strategies.[57] Furthermore, this technique demonstrates its promise as a versatile technology platform, especially in optically sensitive settings like photovoltaics, tactile surfaces, optical lenses, and vehicular windshields.

Methods

Experimental Methods

Hierarchical BCP film preparation. SD123 was synthesized by Avgeropoulos et al. by anionic polymerization with polydispersity PDI = 1.05 [58,59]. SD53 and SD16 (PDI = 1.08) were purchased from PolymerSource. Before the first layer of BCP was deposited onto bare Si substrates, the Si substrates were cleaned with solvents (acetone, toluene, DI water, then nitrogen blow dry).The first BCP was spin-coated from toluene solution on an unetched glass substrate and subsequently annealed in a solvent vapor at room temperature in order to induce microphase separation. Solvent vapor annealing was performed in a 30 cm^3 glass chamber filled with 6 ml of liquid solvent, with the samples supported above the liquid surface and the lid loosely covering the top of the chamber. A binary mixture of solvent vapor produced from toluene:heptane volumetric mixtures in the ratio of 5:1 was used for SD123 solvent annealing, pure toluene vapor was used for SD 53, and pure acetone vapor was used for SD16. After the completion of solvent annealing, the lid of the chamber was slowly removed and the films were dried within 30s at ambient temperature. Film thicknesses were selected to produce a monolayer of in-plane cylindrical PDMS microdomains in a PS matrix, with a thin wetting layer of PDMS forming at the film/ air interface as a result of the lower surface energy of the PDMS block. Subsequently, a CF_4 reactive ion etching (RIE; 5s for SD123 and SD53, and 3s for SD16) was used to remove the PDMS wetting layer, followed by an O_2 RIE (30s for SD123, 22s for SD53, and 12s for SD 16) to remove the PS matrix, leaving a monolayer of oxidized-PDMS microdomains on the substrates. The thickness of the oxidized-PDMS lines was less than about half their width because the O_2 etch converts the PDMS into a silica-like material with a volume reduction as the organic parts (methyl groups) of the PDMS are removed, and the lines formed a fingerprint-like pattern on the substrate lacking long range orientation order. The oxidized-PDMS formed by the oxygen plasma is a robust silica-like material that serves as an insoluble, durable topographical grating pattern. The next layer of self-assembled oxidized-PDMS microdomains was generated by spin-coating another PS-*b*-PDMS BCP directly on top of the lower layer. The sample was subjected to solvent vapor annealing and two-step RIE as described above, leaving a bilayer oxidized PDMS structures on the surface of the substrate. To generate the third layer of self-assembled oxidized-PDMS domains, the BCP film deposition, solvent vapor annealing and two-step

RIE processes were repeated. The process parameters that influence the morphology and alignment angle between BCP layers include the film thickness and annealing, [48,59,60] the amplitude and period of the underlying pattern and its commensurability with the period of the second BCP, and are described in the Supplementary Information, page 4.

Hydrophobizing treatments: The PDMS brush coating was formed by spin-coating a hydroxyl terminated polydimethylsiloxane brush (M_n = 5 kg mol^{-1}, PDI = 1.1, Polymer Source, Inc) onto the multi-layer structure. The sample was baked at 170 ° C under vacuum (20 Torr) for 16 h and was subsequently rinsed by toluene. The grafted PDMS layer is approximately 2 nm thick, measured from spectral reflectometry. The perfluorinated brush was prepared by placing the sample inside a vacuum glass chamber with a 1mL of heptadecafluoro-1,1,2,2,-tetrahydrodecyl trichlorosilane (Gelest, Inc) droplet on a glass slide to create a vapor environment. The fluorination time was 30 min and the fluorinated layer is approximately 1 nm thick. Extended time between etching and coating led to poorer adhesion of the fluorinated layer.

Contact angle measurements, optical and mechanical testing. Droplets of distilled water were applied to the prepared surface, and the static contact angle was measured with a horizontal microscope equipped with a VCA 2000 Optima (AST Products Inc). The mean value was calculated from at least four individual measurements. The optical transmittance spectrum of reference and patterned glass were measured over a wavelength range of 300 – 800 nm, using a UV-Vis spectrophotometer (Perkin Elmer Lambda 1050). For the mechanical tests a high-tack tape (3M VHB Tape 5925 with an adhesion to steel of 3000 N/m) was applied on a sample with SD53 pattern after etching (without the perfluorosilane layer) by rolling a 8 lb. steel roller forward and reverse and subsequently peeled off in a direction perpendicular to the sample surface, as reported by Peng et. al.[56]

Modeling of Topography and Contact Angle. The topography of the hierarchical block copolymer structures was approximated in Fusion 360 CAD software, based on tapping-mode atomic force microscopy (AFM) measurements and prior observations. Examples of experimental measurements of topography are shown in Figures S1(a) and S1(b) and the corresponding model topography in Figure S1(c). The block copolymers SD123, SD53, and SD16 are denoted as layers A, B, and C, with

80nm, 40nm, and 20nm spacing respectively. The topographical oxidized-PDMS features were approximated as half-cylinders with diameter one-half of the period. When one block copolymer layer crossed over another, we introduced a five-point cubic spline at the top of the lower layer, a quarter of the radius down, and the minimum sag at one-half the bottom layer radius, then placed the top hemi-cylinder across this. Any overhanging topography was then extruded to the substrate at a 5° angle from the vertical, mimicking the sidewall taper produced by reactive ion etching.

Next, we swept a surface across the structures to represent the boundary of the water drop, calculating the surface area of the substrate topography above this wetting plane, denoted $\Omega_{SL(h)}$, and the projected area onto the plane beneath, denoted $\Omega_{p(h)}$. Both are functions of the height *h* of the boundary plane above the substrate plane. From these curves, shown in Figure S5, we then calculate the expected wetting angle as a function of height *h* as follows. We begin with the result of Cassie and Baxter[1] shown in equation 1, which gives the predicted wetting angle on an inhomogeneous surface as a function of the wetting angle θ_Y on the solid portion, the fraction f_s of the liquid surface that is in contact with the solid, the contact angle of the liquid interface with air (which is always θ_G =180°) and the fraction of the liquid surface that is in contact with air, f_G. Simplifying these terms according to Calvimontes[49] by recognizing that $f_s + f_G = 1$, $\cos\theta_G = 1$, and $\cos\theta_Y$ is effectively $f_{(h)} r_{SL(h)} \cos\theta_{Y0}$, where θ_{Y0} is the intrinsic contact angle of the flat substrate (determined for example by its brush coating), we obtain equation (2), whose terms $f_{(h)}$ and $r_{SL(h)}$ are defined in equations (3) and (4) and L_m^2 represents the rectangular area of the full simulated region. Equation (2) gives the predicted contact angle as a function of the height of the water contact boundary above the substrate.

$$\cos\phi = f_s cos\theta_Y + f_G \cos\theta_G \quad (1)$$

$$\cos\phi = f_{(h)}(r_{SL(h)} \cos\theta_{Y0} + 1) - 1 \quad (2)$$

$$r_{SL(h)} = \frac{\Omega_{SL(h)}}{\Omega_{p(h)}} \quad (3)$$

$$f_{(h)} = \frac{\Omega_{P(h)}}{L_m^2} \quad (4)$$

When *h* reaches zero, we simply recover the fully-wetted Wenzel regime surface roughness factor *r*. This case is never achieved for hydrophobic surfaces, but for hydrophilic surfaces it provides a check

of our model. With no hydrophobic coating, we measure a contact angle of 40° for the polished glass substrate, and from this we predict a wetting angle of 10° for a single layer of BCP topography, which approximately matches our experimental result of ~13°.

This analysis yields the predicted contact angle as a function of the height of the water-air boundary above the substrate, but the equilibrium value of *h* has to be determined thermodynamically. The analysis of Calvimontes using polygonal maps allows for the prediction of *h* using free energy arguments.[49] Following this approach, we define the total free energy A_{total} in equation (5) where A_{SL} is the interfacial energy contribution of the solid-liquid interface and A_{LG} that of the liquid-air interface, given in Eqs. (6) and (7) respectively. The term $\gamma_{LG}\, L_m^2$ in (6) and (7) represents intrinsic properties of the surface (γ_{LG} is the liquid-air surface energy, γ_{SL} is the solid-liquid surface energy), and does not appear in calculating the equilibrium wetting height. The $(1 - f_{(h)})$ term in Eq. (7) represents the fractional projection of the surface area on the water-air interface, and the $(2 - cos\delta)$ approximates the additional air-water surface area as described in Figure S5. Equations (8-10) show the derivation of δ and are described elsewhere.[49]

$$A_{total} = A_{SL} + A_{LG} \tag{5}$$

$$A_{SL} = -\gamma_{LG}\, L_m^2 \cos(\theta_{Y0})\, f_{(h)} r_{SL(h)} \tag{6}$$

$$A_{LG} = \gamma_{LG}\, L_m^2 \left(1 - f_{(h)}\right)(2 - cos\delta\,) \tag{7}$$

$$\delta_{(h)} = \theta_Y + \alpha_{(h)} - 180° \tag{8}$$

$$r^*_{(h)} = \frac{r_{SL(h)} f_{(h)} - r_{SL(h-\Delta h)} f_{(h-\Delta h)}}{f_{(h)} - f_{(h-\Delta h)}} \tag{9}$$

$$\cos\alpha_{(h)} = \frac{1}{r^*_{(h)}} \tag{10}$$

Once A_{total} is calculated for a range of wetting heights, we then take its derivative with respect to *h*, denoted A^*_{total} which is plotted in Figure S6. The minima of these plots denote the lowest energy configuration of each wetting line, and from this value we can then calculate the expected contact angle from Eq. (2) which is demonstrated graphically in Figure S5. From this procedure, we derived

the contact angles and heights shown in Table 1. This method is appropriate for either of the two hydrophobic treatments used in the experiment, because the difference comes in simply as the θ_{Y0} initial contact angle term which can be varied. In the case of Table 1, we present values calculated for the perfluorosilane treatment.

Author Information

Corresponding Author

*E-mail: caross@mit.edu.

All emails:

Li-Chen Cheng clichen@mit.edu

John Simonaitis johnsimo@mit.edu

Karim Gadelrab karimgad@mit.edu

Mukarram Tahir mtahir@mit.edu

Yi Ding yding@mit.edu

A. Alexander-Katz aalexand@mit.edu

Caroline Ross caross@mit.edu

Author Contributions

L.C. and J.S contributed equally to this paper.

Notes

The authors declare no competing financial interests.

Supporting Information

Supporting Information is available from the Wiley Online Library

Acknowledgements

This study was supported by NSF awards DMR 1606911 and 1246740. J.S acknowledges support from an REU program of the Center for Materials Science and Engineering (award NSF 1419807) at MIT We thank Prof. Apostolos Avgeropoulos for supplying some of the polymers used in the experiments. We also thank the MIT Sandbox program for a seed grant and for their business consulting advice. The shared experimental facilities of the Nano Structures Laboratory and the Center for Materials Science and Engineering (award NSF 1419807) at MIT were used in this work.

Received: ((will be filled in by the editorial staff))
Revised: ((will be filled in by the editorial staff))
Published online: ((will be filled in by the editorial staff))

References

[1] A. B. D. Cassie, S. Baxter, *Trans. Faraday Soc.* **1944**, *40*, 546.

[2] P. G. De Gennes, *Rev. Mod. Phys.* **1985**, *57*, 827.

[3] P. J. Holloway, *Pestic. Sci.* **1970**, *1*, 156.

[4] L. Feng, S. Li, Y. Li, H. Li, L. Zhang, J. Zhai, Y. Song, B. Liu, L. Jiang, D. Zhu, *Adv. Mater.* **2002**, *14*, 1857.

[5] W. Barthlott, C. Neinhuis, *Planta* **1997**, *202*, 1.

[6] C. G. Cong Qian Fang Yan, Ren Lu-quan, *J. Bionic Eng.* **2004**, *1*, 249− 255.

[7] X. Gao, X. Yan, X. Yao, L. Xu, K. Zhang, J. Zhang, B. Yang, L. Jiang, *Adv. Mater.* **2007**, *19*, 2213.

[8] K. Koch, B. Bhushan, W. Barthlott, *Prog. Mater. Sci.* **2009**, *54*, 137.

[9] M. Sun, G. S. Watson, Y. Zheng, J. a Watson, A. Liang, *J. Exp. Biol.* **2009**, *212*, 3148.

[10] T. Wagner, C. Neinhuis, W. Barthlott, *Acta Zool.* **1996**, *77*, 213.

[11] J. Drelich, E. Chibowski, *Langmuir* **2010**, *26*, 18621.

[12] P. Roach, N. J. Shirtcliffe, M. I. Newton, *Soft Matter* **2008**, *4*, 224.

[13] N. Miljkovic, R. Enright, E. N. Wang, *ACS Nano* **2012**, *6*, 1776.

[14] M. E. Callow, J. A. Callow, *Biol.* **2002**, *49*, 10–4.

[15] J. Genzer, A. Marmur, *MRS Bull.* **2008**, *33*, 742.

[16] H. Höcker, *Pure Appl. Chem.* **2002**, *74*, 423.

[17] A. Nakajima, K. Hashimoto, T. Watanabe, *Monatshefte fur Chemie* **2001**, *132*, 31.

[18] S. B. Darling, *J. Appl. Phys.* **2018**, *124*, 030901.

[19] E. Bittoun, A. Marmur, *Langmuir* **2012**, *28*, 13933.

[20] L. Gao, T. J. McCarthy, *Langmuir* **2006**, *22*, 2966.

[21] K. Koch, H. F. Bohn, W. Barthlott, *Langmuir* **2009**, *25*, 14116.

[22] W. Li, A. Amirfazli, *Soft Matter* **2008**, *4*, 462.

[23] Y. Yu, Z. H. Zhao, Q. S. Zheng, *Langmuir* **2007**, *23*, 8212.

[24] R. Fürstner, W. Barthlott, C. Neinhuis, P. Walzel, *Langmuir* **2005**, *21*, 956.

[25] M. Kim, K. Kim, N. Y. Lee, K. Shin, Y. S. Kim, *Chem. Commun.* **2007**, *0*, 2237.

[26] S. S. Latthe, H. Imai, V. Ganesan, C. Kappenstein, A. V. Rao, *J. Sol-Gel Sci. Technol.* **2010**, *53*,

208.

[27] W. Lee, M. K. Jin, W. C. Yoo, J. K. Lee, *Langmuir* **2004**, *20*, 7665.

[28] P. A. Levkin, F. Svec, J. M. J. Fréchet, *Adv. Funct. Mater.* **2009**, *19*, 1993.

[29] X. Y. Ling, I. Y. Phang, G. J. Vancso, J. Huskens, D. N. Reinhoudt, *Langmuir* **2009**, *25*, 3260.

[30] A. Mills, A. Lepre, N. Elliott, S. Bhopal, I. P. Parkin, S. A. O'Neill, *J. Photochem. Photobiol. A Chem.* **2003**, *160*, 213.

[31] M. J. Tallman, C. Santner, R. B. Miller, *Durable Hydrophobic Surface Coatings Using Silicone Resins*, **2008**, U.S. Patent No. 7,344,783.

[32] H. Zhang, Y. Li, Z. Lu, L. Chen, L. Huang, M. Fan, *Sci. Rep.* **2017**, *7*, 3.

[33] L. Wang, J. Yang, Y. Zhu, Z. Li, T. Sheng, Y. M. Hu, D. Q. Yang, *Colloids Surfaces A Physicochem. Eng. Asp.* **2016**, *497*, 16.

[34] C. A. Foss, G. L. Hornyak, J. A. Stockert, C. R. Martin, *J. Phys. Chem.* **1994**, *98*, 2963.

[35] J. Bravo, L. Zhai, Z. Wu, R. E. Cohen, M. F. Rubner, *Langmuir* **2007**, *23*, 7293.

[36] R. G. Karunakaran, C. H. Lu, Z. Zhang, S. Yang, *Langmuir* **2011**, *27*, 4594.

[37] A. Nakajima, K. Hashimoto, T. Watanabe, K. Takai, G. Yamauchi, A. Fujishima, *Langmuir* **2000**, *16*, 7044.

[38] J. N. L. Albert, T. H. Epps, *Mater. Today* **2010**, *13*, 24.

[39] F. S. Bates, G. H. Fredrickson, *Annu. Rev. Phys. Chem.* **1990**, *41*, 525.

[40] C. J. Hawker, P. Thomas, *MRS Bull.* **2005**, *30*, 952.

[41] A. Telecka, T. Li, S. Ndoni, R. Taboryski, *RSC Adv.* **2018**, *8*, 4204.

[42] J. T. Han, X. Xu, K. Cho, *Langmuir* **2005**, *21*, 6662.

[43] S. Krishnamoorthy, Y. Gerbig, C. Hibert, R. Pugin, C. Hinderling, J. Brugger, H. Heinzelmann, *Nanotechnology* **2008**, *19*, 1.

[44] N. Zhao, Q. Xie, L. Weng, S. Wang, X. Zhang, J. Xu, *Macromolecules* **2005**, *38*, 8996.

[45] A. Checco, A. Rahman, C. T. Black, *Adv. Mater.* **2014**, *26*, 886.

[46] A. Baruth, M. D. Rodwogin, A. Shankar, M. J. Erickson, M. A. Hillmyer, C. Leighton, *ACS Appl. Mater. Interfaces* **2011**, *3*, 3472.

[47] S. Xiao, X. Yang, E. W. Edwards, Y. H. La, P. F. Nealey, *Nanotechnology* **2005**, *16*, S324.

[48] M. A. Hartney, J. N. Chiang, D. W. Hess, D. S. Soane, *Appl. Phys. Lett.* **1989**, *54*, 1510.

[49] A. Calvimontes, *Soft Matter* **2014**, *10*, 8308.

[50] A. T. K. G., S. M. Nicaise, K. R. Gadelrab, A. Alexander-Katz, C. A. Ross, K. K. Berggren, *Nat. Commun.* **2016**, *7*, DOI 10.1038/ncomms10518.

[51] J. G. Son, A. F. Hannon, K. W. Gotrik, A. Alexander-Katz, C. A. Ross, *Adv. Mater.* **2011**, *23*, 634.

[52] Y. Tsori, D. Andelman, *Eur. Phys. J. E* **2001**, *5*, 605.

[53] D. Helmer, N. Keller, F. Kotz, F. Stolz, C. Greiner, T. M. Nargang, K. Sachsenheimer, B. E. Rapp, *Sci. Rep.* **2017**, *7*, 1.

[54] R. G. Karunakaran, C.-H. Lu, Z. Zhang, S. Yang, *Langmuir* **2011**, *27*, 4594.

[55] L. Xu, J. He, *Langmuir* **2012**, *28*, 7512.

[56] C. Peng, Z. Chen, M. K. Tiwari, *Nat. Mater.* **2018**, *17*, 355.

[57] Y. Si, Z. Guo, *Nanoscale* **2015**, *7*, 5922.

[58] V. Bellas, H. Iatrou, N. Hadjichristidis, *Macromolecules* **2000**, *33*, 6993.

[59] L. C. Cheng, W. Bai, E. Fernandez Martin, K. H. Tu, K. Ntetsikas, G. Liontos, A. Avgeropoulos, C. A. Ross, *Nanotechnology* **2017**, *28*, DOI 10.1088/1361-6528/aa61c9.

[60] W. Bai, A. F. Hannon, K. W. Gotrik, H. K. Choi, K. Aissou, G. Liontos, K. Ntetsikas, A. Alexander-Katz, A. Avgeropoulos, C. A. Ross, *Macromolecules* **2014**, *47*, 6000.

TOC Text

smll.201905509R1

A robust and transparent silica-like coating created through block copolymer self-assembly imparts superhydrophobicity to a surface through its hierarchical multilevel structure. A model based on the hierarchical topography calculates the wetting angle and optimizes the superhydrophobicity, in agreement with the experimental trends, and explains how the superhydrophobicity arises through a combination of roughness at different lengthscales.